Antenna Miniaturization Using Slow Wave Enhancement Factor from Loaded Transmission Line Models

Pei-Ling Chi, *Student Member*, *IEEE*, Rod Waterhouse, *Senior Member*, *IEEE*, and Tatsuo Itoh, *Life Fellow, IEEE*

Abstract—**Miniaturization of slow wave antennas exploiting the slow wave enhancement factor is presented. The printed antennas are periodically loaded with shunt capacitors to slow down the guided wave in the structures. In this paper, the loaded unit cell of the equivalent transmission line model is utilized to extract the slow wave enhancement factor, the ratio of the loaded to the unloaded propagation constants of the wave in the antennas. From this model, the slow wave enhancement factor of a loaded antenna agrees very well with the miniaturization factor, and therefore load parameters in the circuit model can be readily obtained when a specific size reduction is attempted. This claim was substantiated by demonstrating two small radiators, a high-frequency (HF) slot-loop antenna and a planar inverted F antenna (PIFA), to achieve the desired size reductions. Experimental results show that both of the antennas demonstrate greater than ten-times size reduction from their unloaded counterparts at the expense of the degraded gains and impedance bandwidths. Specifically, the loaded slot loop presents the predicted gain and measured bandwidth on the order of -34.9 dBi and 0.38% for VSWR≤ 2, respectively. Therefore, a matching network derived from filter design techniques is proposed to increase the antenna bandwidth so that a measured fractional bandwidth of 1.78% is achieved. The slot loop combined with the impedance matching circuit occupies a footprint size of $0.031\lambda_0 \times 0.017\lambda_0$ at the operating frequency. On the other hand, the measured radiation gain and bandwidth of the loaded PIFA are reduced to -22.6 dBi and 0.15% for VSWR≤ 2, respectively, with a footprint of $0.013\lambda_0 \times 0.018\lambda_0$ at the operating frequency.**

Index Terms—**Periodic structure, slow wave, small antenna, transmission line model.**

I. Introduction

As communication systems equipment is downsized substantially, their integral elements need to be reduced accordingly. Antennas usually occupy substantial real estate in the front-end modules, indicating that their sizes are critical to the overall volume. This is particularly crucial if the operating frequency is low such as in the high frequency (HF) band. There have been many techniques employed to attempt size reduction. The application of high dielectric constant substrates to enhance the effective permittivity is the easiest way to reduce the guided wavelength and thus the physical size of antennas [1-3]. Similarly, magnetic materials of high permeability can be utilized for size reduction [4]. In [5, 6], footprints are reduced with particular antenna layouts, such as folded and meandered configurations. These complicated antenna structures are not straightforwardly determined, however, and they involve time-consuming parametric optimization. One class of miniaturization is to seek for particular materials of higher-order or controllable dispersion relations. For example, degenerate band edge crystals exhibit 4^{th} order ω-β curves at the band edges and thus resonances can be reduced to lower frequencies [7]. In addition, artificial left-handed metamaterials have been found capable of tailoring the dispersion characteristics to desired frequency responses by optimizing the constituent unit cells, which lend themselves to the application of miniaturization [8, 9].

Alternatively, antennas can be modeled as transmission lines, allowing the transmission line theory to be applied. In this scenario, a physically short transmission line can exhibit a considerable electrical length by increasing the equivalent inductance or/and capacitance per unit length. This results in a slow wave structure with an enhanced propagation constant. Examples of increasing the effective propagation constants are the inductive or capacitive elements loaded to the radiating elements [10-13] and the uniplanar compact photonic bandgap transmission line [14]. Slot-loop antennas have dipole-like radiation characteristics but provide wider impedance bandwidths [15-18]. Furthermore, capacitive loading is mechanically easier by mounting chip capacitors across the slot. By taking this advantage, a preliminary work for a slow wave slot loop has already been reported [19], where shunt capacitors were distributed periodically along the slot loop and the loaded transmission line model characterizing the slow wave antenna was briefly addressed. By the same token, the transmission line model was used to investigate the input impedance of a wideband spiral antenna [20]. In this paper, complete characterization of the developed antennas is carried out by the periodically loaded transmission line models. The load effect on the propagation constant, characteristic impedance, and appearance of the stop-band region versus the load parameters

Manuscript received March 31, 2009. This work was supported by the ONR STTR Phase II Program, Topic#: N06-T032.

P. -L. Chi and T. Itoh are with the Department of Electrical Engineering, University of California at Los Angeles, Los Angeles, CA 90095, USA (e-mail: peiling@ ee.ucla.edu).

R. Waterhouse is with the Pharad LLC, 797 Cromwell Park Drive, Suite V, Glen Burnie, MD 21061, USA (e-mail: rwaterhouse@ pharad.com).

are studied thoroughly. By exploiting the transmission line model, the calculated slow wave enhancement factor, the ratio of the loaded to the unloaded propagation constants, agrees very well with the miniaturization factor. Subsequently, antennas can be specifically miniaturized using those load parameters with the desired slow wave enhancement factor. In this paper, the developed capacitor-loaded HF slot-loop antenna and PIFA are significantly miniaturized based on this methodology and are capable of operating at one-eleventh the frequencies of the unloaded antennas. Antenna gains and impedance bandwidths are, however, deteriorated as a result of miniaturization. The predicted antenna gain and measured bandwidth of the loaded slot loop are -34.9 dBi and 0.38% at 24 MHz, respectively. In addition, the measured radiation gain and bandwidth of the loaded PIFA are reduced to -22.6 dBi and 0.15% for VSWR≤ 2, respectively. Thereby, the trade-off of the radiation efficiency versus size reduction factor is investigated as well.

The fundamental lower bound of the radiation quality factor (Q) derived by Chu indicates that the maximum impedance bandwidth is limited and can be increased at the expense of the efficiency or the system complexity. In the present paper, two impedance matching networks are developed for the miniaturized slot-loop antenna to overcome the issue of impedance mismatch. The first network is constructed based on an L section matching circuit and is narrowband. On the other hand, an impedance matching network derived from filter design techniques is proposed to increase the antenna impedance bandwidth. The underlying principle of realizing this matching circuit is to regard the antenna as a resonant load around resonance, and the elements in the matching circuit can be determined by specifications as in filter designs [21]. Utilizing the virtues of the compactness and better performance of surface-mount chip components at UHF frequencies and lower, the proposed HF antenna with the filter-type matching circuit avoids a complicated layout [22] and its fractional bandwidth is substantially improved to 1.78% for VSWR≤ 2 in the experiment while occupying a small area $0.031\lambda_o \times 0.017\lambda_o$, where λ_o is the free space wavelength at resonance.

The configuration of this paper is as follows. In Section II, development of the equivalent transmission line is described along with the circuit characterization by giving an example. In the end, a design procedure that enables miniaturized antennas to be achieved is outlined. In Section III we present our antenna examples of how we applied the proposed slow wave procedure to printed antennas: a slot-loop antenna and PIFA. Simulated and measured results are given. In this section we also explain the procedure used to enhance the $|S_{11}|$ bandwidth of these electrically small antennas. Section IV provides a summary of the results presented.

II. Design Procedure of a Slow-Wave Based Miniaturized Antenna with Flexible Size Reduction

In the present paper, slow wave structures periodically loaded with shunt capacitors are employed as the mechanism for antenna miniaturization with regards to the implementation convenience for the proposed antennas. When depicted in a dispersion (k-β) diagram, a capacitor-loaded slow wave structure represents a line underneath the air line $k=\beta$ and has a propagation mode with propagation constant β larger than the propagation constant β_0 of the unloaded (host) structure, as shown in Fig. 1 along with an inset of the unit cell. Please note that the dispersion curve for the unloaded structure can be non-linear, which is the case when dispersive transmission lines are considered as the host lines, such as the microstrip

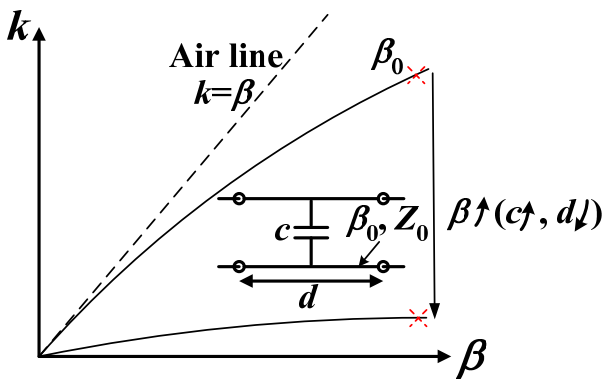

Fig. 1. The illustration of a capacitor-loaded slow wave structure in the k-β diagram.

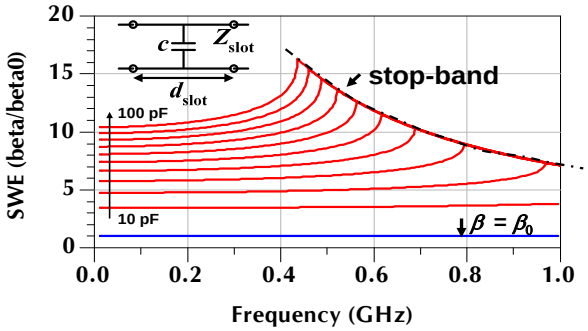

(a)

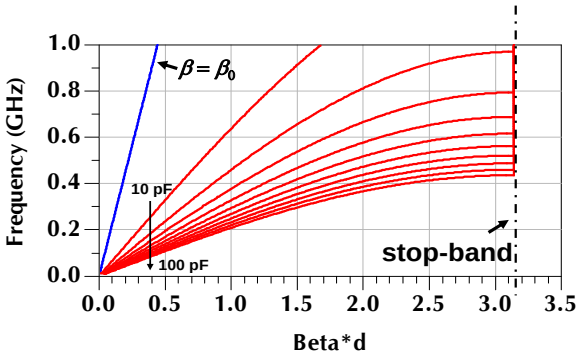

(b)

Fig. 2. (a) The SWE (β/β_0) versus loaded shunt capacitance for the capacitor-loaded unit cell. The capacitance sweep is from 10 pF to 100 pF with a fixed Z_{slot}= 75.44 Ω and a load interval d_{slot}/λ_g= 7.6 degrees at 300 MHz, (b) the corresponding frequency responses of the capacitor-loaded unit cell versus βd.

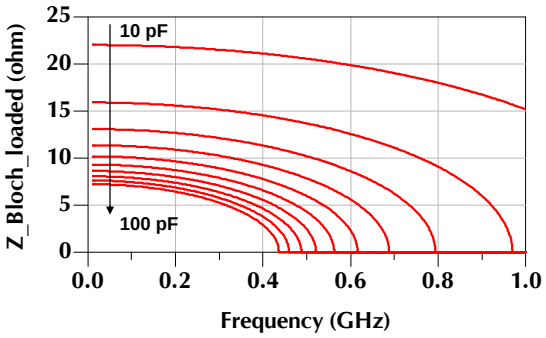

Fig. 3. Variation of the Bloch impedance for the capacitor-loaded unit cell. The capacitance sweep is from 10 pF to 100 pF with a fixed Z_{slot}= 75.44 Ω and a load interval d_{slot}/λ_g= 7.6 degrees at 300 MHz.

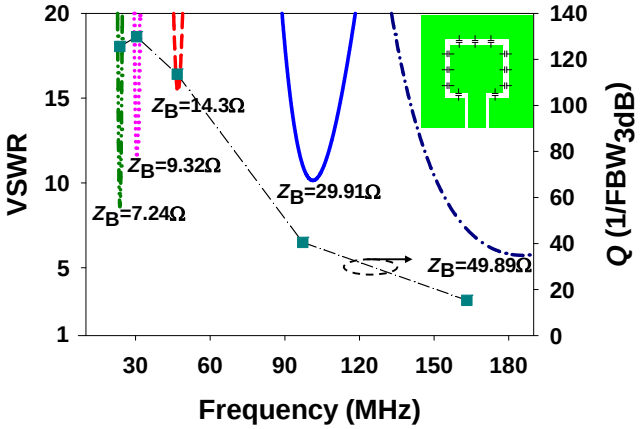

Fig. 4. Calculated input VSWRs of the CPW-fed capacitor-loaded slot-loop antennas (with an inset) with 5 cases of different Z_Bs. The corresponding quality factors (*Q*s) are included in the figure. The slot width, load period, substrate thickness and dielectric constant of the antennas are 2 mm, 20 mm, 0.508 mm, and 4.5, respectively.

lines and slot lines [23]. The propagation constant β is a function of the load capacitance and period for a given host transmission line and as the entire structure is increasingly loaded by larger capacitance or/and smaller period, the corresponding β is increased toward the abscissa and the loaded structure is electrically longer despite the same physical length.

The loaded transmission line model with periodic boundary conditions is applied to characterize the behavior of a periodic loaded antenna and developed in the Advanced Design System (ADS). Please note that the loaded propagation constant β is obtained from the ABCD matrix of a loaded unit cell, where the ABCD matrix characterizes the unique feature of a particular unit cell and therefore it is independent of the termination loads. Furthermore, when the periodicity is well maintained, the unit-cell model (as the inset shown in Fig. 1) can fully represent the property of the loaded structure, such as its propagation constant. Therefore, the characteristic impedance Z_0 of the host transmission line, the load interval *d*, and the load capacitance *c* need to be determined. The characteristic impedance Z_0 is determined by two steps. First, a particular transmission line best suited to describe the radiating element is assigned as the host transmission line. Second, the impedance is determined by antenna structural and material parameters. For example, a slot-loop antenna is represented by a slot line with Z_0 depending on the slot width and substrate. In addition, the load interval and load capacitance are used as parameters to engineer the loaded propagation constant β.

An example is given here. The slow wave enhancement factor (SWE), defined as the ratio of the loaded to the unloaded propagation constants as follows

$$\mathrm{SWE} = \frac{\beta}{\beta_0}, \qquad (1)$$

is of particular interest due to its proportionality to the miniaturization factor. Two approaches, viz. increasing the load capacitance and decreasing the load interval, are found effective to increase the propagation constant β, or the SWE as indicated in [24]. Fig. 2 investigates the SWE with respect to the load capacitance of a capacitor-loaded unit cell. The characteristic impedance Z_{slot} of this unit cell is determined from a 2 mm wide slot line on a substrate of thickness 0.508 mm and ε_r= 4.5, and thus is approximated to be 75.44 Ω from the numerical equations provided in [25]. In addition, the electrical length of the unit cell is fixed at 7.6 degrees at 300 MHz (d_{slot}/λ_g). As the capacitance *c* is increased from 10 pF to 100 pF, the SWE is increased as expected and the unity ($\beta=\beta_0$) corresponds to the unloaded case (*c*=0). It is observed from Fig. 2(a) the rate of this enhancement is, however, diminished as the capacitance is continually increased. In addition, the stop bands are encountered as the structure is increasingly loaded when the SWE is inversely proportional to the frequency. These stop bands can be easily verified and occur at frequencies where the product βd is equal to π as shown in Fig. 2(b). For implementation, one should avoid stop-band occurrences in the operational range of interest. The Bloch impedance Z_B of the same example is also investigated in Fig. 3 and is continuously decreased at a retarded rate as the capacitive load is increased. From the transmission line theory, the reduced impedance is expected as a result of the increase in the effective capacitance per unit cell (length). Moreover, the Bloch impedances approach zero at frequencies where the respective stop bands occur. In order to compensate the mismatch factor, a series inductance should be commensurately added as mentioned in [20].

In order to optimize antenna performance, the influence of the Bloch impedance (of a unit cell) on the input impedance is studied. Corresponding to the capacitor-loaded unit cell of the slot line discussed previously, a slot-loop antenna fed by the 50 Ω coplanar waveguide (CPW) is used. Input VSWRs of different Bloch impedances loops were calculated by full-wave simulations in the High Frequency Structure Simulator (HFSS). By periodically loading the slot loop with 1.2 pF, 5 pF, 25 pF, 60 pF, and 100 pF capacitors at an interval of 20 mm, Bloch impedances Z_Bs of 49.89 Ω, 29.91 Ω, 14.3 Ω, 9.32 Ω, and 7.24

TABLE I
FULL-WAVE MINIATURIZATION FACTOR VERSUS SWE FOR THE LOADED SLOT-LOOP ANTENNA

Loaded capacitance c (pF)	Miniaturization factor (unloaded frequency/ loaded frequency in MHz)	SWE
1.2	1.6 (255.2/163.75)	1.5
5	2.6 (255.2/97.25)	2.5
25	5.5 (255.2/46.7)	5.3
60	8.4 (255.2/30.4)	8.8
100	10.8 (255.2/23.65)	10.4

Ω are generated. As shown in Fig. 4, the impedance matching is not significantly improved as the Bloch impedance approaches 50 Ω, which manifests the effect of the excitation mechanism. In addition, antenna miniaturization is observed from the increased radiation quality factor (Q), defined as the inverse of the 3-dB impedance fractional bandwidth (half-power bandwidth), as the Bloch impedance Z_B is gradually reduced. Most importantly, the miniaturization factor, as the resonance frequency of the unloaded antenna compared to the respective resonance frequencies of the loaded antenna in Fig. 4, coincides very well with the SWE obtained from the developed circuit model. TABLE I compares the miniaturization factors with SWEs based on the circuit model. Excellent agreement is achieved which implies the feasibility of the developed transmission line model. Practically, when a particular size reduction using the loaded slow wave antennas is attempted, the required structure can be implemented by employing the corresponding load parameters. In order to facilitate fabrication of the antenna prototype of interest (the slot-loop and PIFA), only shunt capacitors are considered in the present paper. The design procedure of a loaded slow wave antenna with specific miniaturization is as follows.

Step 1) Establish the equivalent loaded unit cell for the loaded antenna. Three parameters involved in the model are the characteristic impedance Z_0 of the host transmission line, the unit-cell electrical length d/λ_g, and the shunt capacitance c.

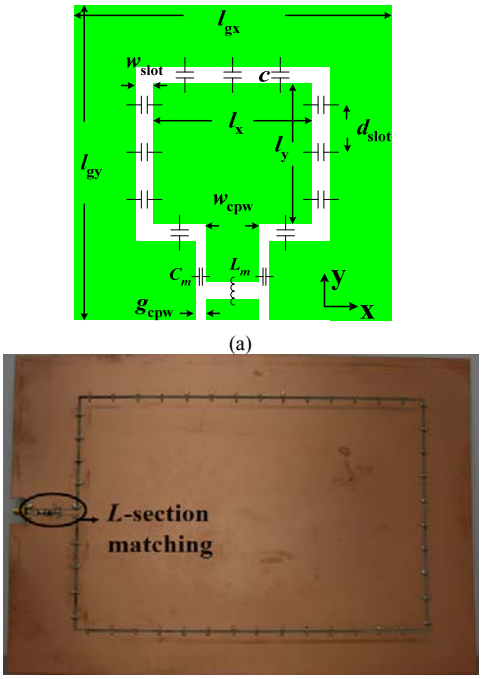

Fig. 5. (a) The configuration of the proposed capacitor-loaded HF slot-loop antenna with the L-section matching circuit. (b) Photograph of the fabricated antenna.

Step 2) Investigate the SWE as functions of the load parameters. The SWE is obtained by taking the ratio of the loaded to the unloaded propagation constants of the unit-cell circuits.

Step 3) Employ those load parameters resulting in the desired SWE. Disregard those solutions with stop bands near or at frequencies of interest.

Step 4) Consider other fabrication factors. For example, a small load period would increase the fabrication difficulty, leading to fabrication errors.

In the following section, two miniaturized antennas based on

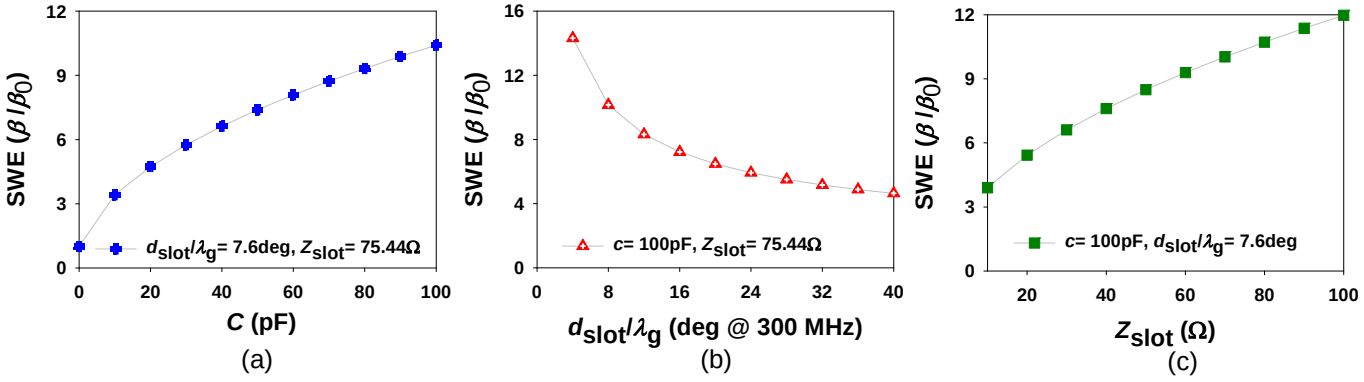

Fig. 6. SWE investigation for the capacitor-loaded HF slot-loop antenna (a) SWE vs. load capacitance (b) SWE vs. load period (c) SWE vs. characteristic impedance of the slot line.

the loaded slow wave structure are demonstrated as examples using the SWE approach.

III. Antenna Miniaturization Using the SWE Approach

A. The Capacitor-Loaded and Miniaturized HF Slot-Loop Antenna with L-Section Matching Circuit

Using predicted load parameters from the unit-cell circuit model, a miniaturization of the capacitor-loaded HF slot-loop antenna is demonstrated as follows. Furthermore, two matching networks are presented to improve the impedance performance of the small slot-loop antenna, including an *L*-section matching circuit here and an advanced four-pole matching network based on the filter design techniques in Section III-B. The antenna prototype used for miniaturization is a λ slot loop. Applying the slot line model to this slot loop, the characteristic impedance Z_{slot} for the slot line can be determined from the slot-loop width w_{slot}, substrate information, and the operating frequency. In this example, shunt capacitors are periodically distributed along the aperture. Fig. 5 illustrates the configuration of the proposed loaded HF slot-loop antenna. The associated unit-cell model can be referred to the inset in Fig. 2(a). Employing those particular values (w_{slot}= 2 mm and an ε_r= 4.5 substrate of thickness 0.508 mm) exemplified in Section II, the SWEs with respect to the load capacitance c, load period d_{slot}/λ_g, and slot line Z_{slot} are investigated in Fig 6. Each investigation is performed by one variable sweep at a time while the rest are kept as labeled. As expected, the SWE increases when the structure is increasingly loaded (with increased load capacitance or decreased load interval). Furthermore, the SWE becomes larger with the host characteristic impedance. The shunt capacitance c= 100 pF, d_{slot}/λ_g= 7.6 degrees at 300 MHz (20 mm), and Z_{slot}= 75.44 Ω corresponds to a SWE of 10.4 as can be observed in the figure. These values will be used for fabrication later. In viewpoint of miniaturization design, the slot width is able to engineer the SWE through the corresponding characteristic impedance Z_{slot} of the loop. At around several hundred MHz the wider slot width corresponds to lower characteristic impedance, and therefore the lower miniaturization effectiveness. The input match of the antenna is not, however, benefited by choosing a particular slot width. This is shown already in Section II where the input VSWR of a 50 Ω Bloch impedance loop is not satisfactory. In addition, from the antenna figure of merit, the radiation efficiency is almost unchanged with respect to the slot width. Therefore, in the present paper, the slot width of the loop is chosen at the convenience of capacitor placement.

Fig. 5(b) shows the photograph of the proposed capacitor-loaded HF slot-loop antenna combined with the *L*-section matching circuit. The slot-loop antenna was fed by CPW and built on an Arlon AR 450 substrate with ε_r=4.5 and thickness 0.508 mm. The unloaded slot-loop antenna was designed to have one wavelength resonance at 255.2 MHz and is able to operate at high frequency (HF: 3-30 MHz) after proper size reduction. Here, the Vishay/Dale 1206 SMD 100 pF lumped capacitors are mounted across the slot and the dimensions for the fabricated slow wave slot-loop antenna are as follows (see Fig. 5(a)): l_x= 190 mm, l_y= 284 mm, l_{gx}= 264 mm, l_{gy}= 382.8 mm, w_{slot}=2 mm, d_{slot}= 20 mm, w_{cpw}= 4.4 mm, and g_{cpw}= 0.2 mm. The measurement was taken with the Anritsu MS2034A vector network analyzer. Fig. 7 shows the measured and simulated $|S_{11}|$ for the loaded slot-loop with and without the matching circuit. As observed from the figure, the measured responses agree well with the simulated results. Impedance matching is significantly improved due to the *L* matching circuit where a series inductance L_m=864 nH and a shunt capacitance C_m=29.2 pF are used. The matched slot loop has a measured $|S_{11}|$ of -12.04 dB at 24 MHz with a fractional bandwidth 0.38% for VSWR≤ 2, which is considerably reduced as expected from its unloaded counterpart with a bandwidth 7.07%. Lumped elements are exploited for the compactness and easy implementation of the matching network, which avoids configuring space-consuming and complicated matching patterns especially in HF bands. From experimental results, the one wavelength resonant frequency was effectively reduced from the 255.2 MHz to 24 MHz, showing a size reduction of 10.6. Compared to the predicted SWE of 10.4, this result confirms the applicability using SWEs in designs of antenna miniaturization.

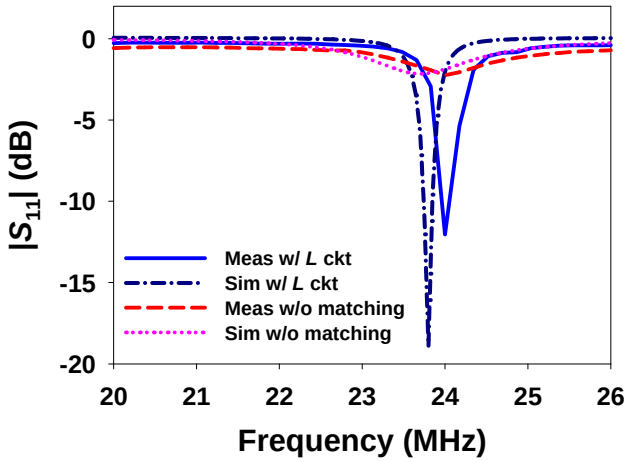

Fig. 7. Measured and calculated $|S_{11}|$ of the loaded HF slot-loop antenna with and without the *L*-section matching circuit.

Due to the limited facilities, our chamber can only accommodate radiation measurements down to 300 - 400 MHz. Therefore only the calculated radiation gains of the proposed loaded HF slot-loop antenna with matching circuits are presented. It should be noted that the predicted and measured results for the loaded PIFA (see Section III-C) are in good agreement. Fig. 8 shows the predicted radiation gains of the loaded antenna where dipole-like radiation patterns are observed as shown in [19]. The E and H principal planes of this antenna are parallel to the yz and xz planes in Fig. 5(a) respectively. From simulated results, the maximum radiation gain for the loaded slot-loop antenna with the *L* matching circuit is -34.9 dBi (with radiation efficiency η_r= 0.08). This is resulted from the considerable size reduction compared to the unloaded antenna. As a fundamental trade-off exists between size reduction and antenna radiation efficiency, a compromise

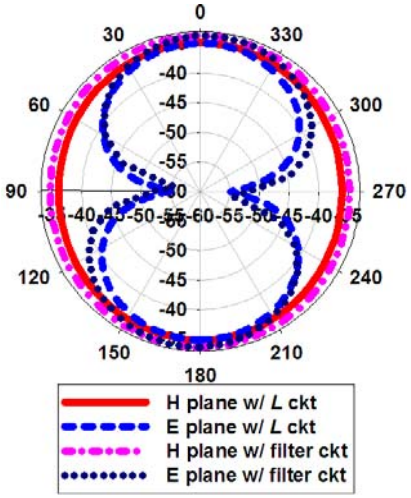

Fig. 8. Calculated radiation gains of the loaded HF slot-loop antennas with the *L*-section and four-pole filter-type impedance matching networks, respectively.

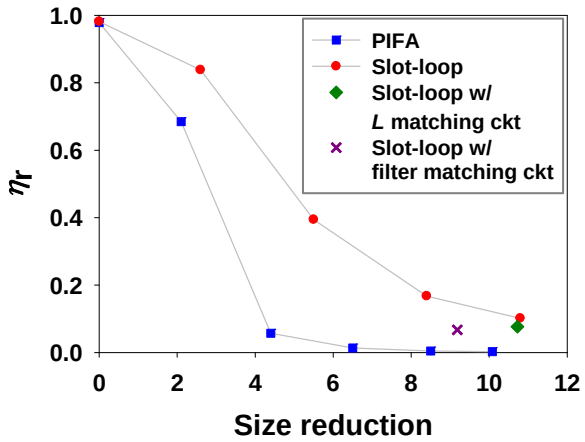

Fig. 9. Predicted radiation efficiency η_r with respect to the size reduction.

needs to be made when considering size reduction. Fig. 9 establishes the HFSS calculated radiation efficiency with relation to the size reduction for both small antennas in this paper. The effect of the matching networks on the radiation efficiency of the HF slot-loop antenna is investigated as well. Both the conductor and dielectric losses are considered in our full-wave simulation. The lumped-element loss is not included here for two reasons. First, based on the comparison at the frequencies of interest (at around 400 MHz for the capacitors used in the loaded PIFA and at around 25 MHz for all the lumped elements used in the loaded slot-loop) the measured responses of the lumped elements are in good agreement with those of the respective ideal models. Second, to the best of the authors' knowledge, the measured *S*-parameters cannot be embedded into the HFSS simulation environment. The equivalent loss resistance needs to be extracted from the measured *S*-parameters in order to simulate the behavior of a non-ideal lumped element in HFSS. Essentially, the radiation efficiency of the loaded HF antenna decreases with size reduction as electrically smaller antennas are well known for the poor radiation capability. Despite the good agreement between lossless models and measured results of lumped elements, the measured efficiency of the HF slot-loop antenna may suffer more losses (as compared to the predicted efficiency) from the fabrication error and the possible lumped-element loss provided that the nearby cable radiation is perfectly prevented (see Section III-C). Furthermore, when the *L*-section impedance matching circuit is used, the radiation efficiency is reduced further. Higher density of current distribution on the metal surface around lumped elements (of matching networks) was observed in the model, which invokes increased conductor loss. Several approaches can be applied to improve the radiation efficiency. For example, antennas built on thicker substrates are prone to radiate [26]. Similar to the monopole concept, antennas backed with large ground planes are able to increase the forward directivity [27]. Moreover, stacked structures composed of antenna substrates mounted with a high dielectric superstrate can be employed [28-30]. All of the above methods, however, inevitably lead to bulky antenna structures and increasing fabrication expenses.

Due to the large wavelength at HF frequencies, conventional man-portable antennas that can operate in this band typically have low gains. For example, a 10 foot monopole has a gain of approximately -24 dBi at 2 MHz [31]. For applications such as short range communications (less than 0.5 miles) and medium range communications (less than 12 miles) these levels of gain are acceptable. A new application currently under consideration for HF communications is for disaster recovery units. Here HF communications are being considered because of the advantageous propagation characteristics of this frequency range through concrete and other building materials as well as tunnels, or obstructed passages. Although exactly fair comparison is not possible, it is noted that the proposed slot-loop antenna has a lower radiation gain as compared to that of a size-comparable monopole antenna backed with the same ground plane dimensions as our antenna at 24 MHz. Our further investigation on the gain shows that the capacitive loading in our structure creates the current discontinuity and introduces the additional ohmic loss, deteriorating the radiation efficiency. Nevertheless, due to the planar nature, the loaded slot-loop antenna provides higher portability and integrability with other components.

B. The Proposed Filter-Type Matching Network for the Bandwidth-Improved HF Slot-Loop Antenna

In last subsection, an *L*-section matching circuit improved the impedance matching significantly. However, the instantaneous bandwidth is greatly limited due to the inherent property of the electrically small antennas. In order to effectively increase the bandwidth, in this subsection, the filter design technique [21] is applied to the realization of an increased bandwidth matching network for the miniature slot-loop antenna.

The underlying principle of implementing antenna matching circuits based on the filter design approach is to consider the antenna to be a resonant load around resonance. In many

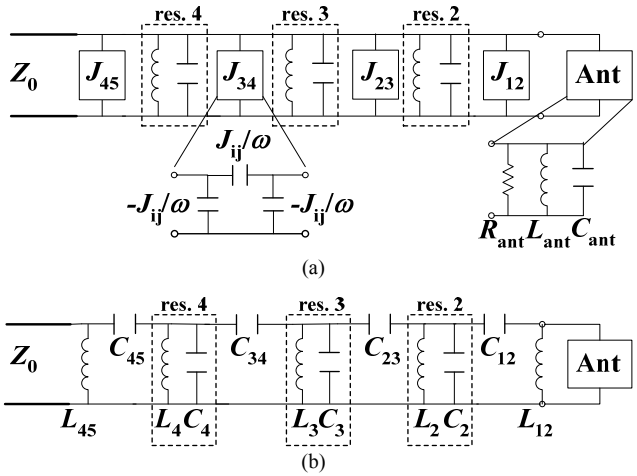

Fig. 10. (a) Illustration and (b) corresponding implementation of the impedance matching network using filter design techniques [21] for the loaded HF slot-loop antenna. Four-pole prototype matching circuit (including the antenna) is used in this case.

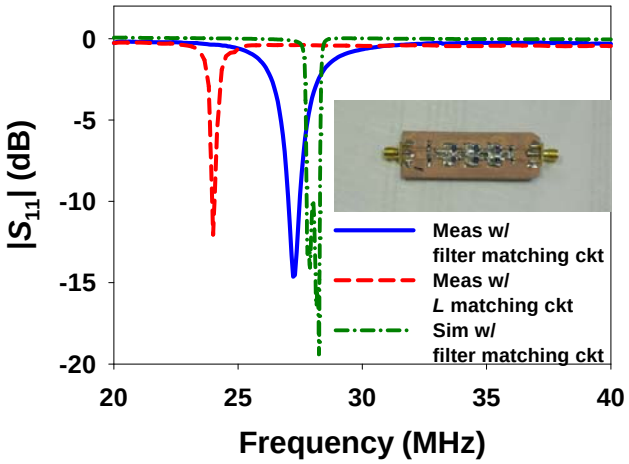

Fig. 11. Measured and calculated $|S_{11}|$ of the loaded HF slot-loop antenna with the filter-type impedance matching network. The measured $|S_{11}|$ of the HF slot-loop antenna with *L*-section matching circuit is included for comparison.

TABLE II
LUMPED-ELEMENT PARAMETERS IN THE MATCHING CIRCUIT FOR THE LOADED SLOT-LOOP ANTENNA

L_{12}=75 nH	C_{12}=29.4 pF	C_2=959 pF	L_2=32 nH
C_{23}=11.7 pF	C_3=971 pF	L_3=32 nH	C_{34}=17.4 pF
C_4=930.6 pF	L_4=32 nH	C_{45}=52 pF	L_{45}=1.2 μH

situations, antennas can be approximated as series or parallel resonators over the frequency range of interest. Therefore, elements in the matching circuit are conceived as the remaining components in a band-pass filter and can be determined by the circuit order *n*, the maximum in-band attenuation $(L_A)_{max}$, and the equal-ripple fractional bandwidth $\Delta\omega$. Using filter-like impedance matching circuits enables a considerable bandwidth improvement as desired. It is found, however, that the high-*Q* feature of the small antenna mainly restrict the capability. In addition, the degraded radiation efficiency of the HF slot-loop due to the lumped elements in filter-type matching circuit will be discussed later.

The illustration of the impedance matching network under consideration is exhibited in Fig. 10(a). For the slot-loop antenna, it is observed that around resonance the input admittance locus of the antenna varies along a constant conductance circle and therefore is best suited to be modeled as a parallel resonator. In order to compensate for the high-*Q* of the antenna, a filter order *n* equal to 4 is chosen and further increase in *n* is found with diminishing bandwidth improvement. The admittance inverters J_{ij}s are introduced between stages to allow for input impedance match to Z_0, usually 50 Ω. Of many admittance inverter realizations, the particular circuit shown as the inset in Fig. 10(a) is used. Note that the negative shunt capacitance at both sides can be absorbed into the nearby capacitance in resonators or equivalently equated to an inductance. In other words, the equivalent L_{ij} in place of the negative shunt C_{ij} $(-J_{ij}/\omega)$ is

$$L_{ij} = \frac{1}{\omega_0^2 C_{ij}} = \frac{1}{\omega_0 J_{ij}}, \quad (2)$$

where the resonant frequency ω_0 of the antenna is used for narrowband approximation. Eventually, the corresponding implementation of the impedance matching network is of the configuration shown in Fig. 10(b). The capacitances C_{12}, C_{23}, C_{34}, and C_{45} result from the corresponding capacitances in the center of each inverter realization. The inductances L_{12} and L_{45} come from the negative capacitance equivalences as aforementioned. Furthermore, the values of C_2, C_3, and C_4 need to be adjusted for nearby negative shunt capacitances. The design specifications of this filter-like matching circuit are as follows: n= 4, $(L_A)_{max}$= 0.1 dB, in-band ripple level $(L_A)_{max}$-$(L_A)_{min}$= 0.04 dB, and $\Delta\omega$ (0.04 dB)= 1.64%. Based on these specific terms, lumped-element parameters in the matching network are determined and can be found using the look-up diagrams in [21]. TABLE II lists the element values. We sourced the lumped components for the matching circuit from Mouser Electronics Inc. The big capacitance or inductance was made up from several smaller values. Otherwise, exact (or close enough to) lumped element as shown in TABLE II was mounted. Thereby, 17 lumped-element values are employed in the matching network and as follows: Murata 0805 SMD Monolith 2.4 pF, Xicon 1206 Ceramic Chip 470 pF, Vishay/Vitramon 1206 Ceramic 430 pF, Kemet 1206 SMD Ceramic 51 pF, Vishay/Vitramon 1206 Ceramic 33 pF, Kemet 1206 SMD Ceramic 27 pF, Murata 0805 SMD Monolith 16 pF, Vishay/Vitramon 1206 Ceramic 15 pF, AVX 1206 SMD Ceramic 0.5 pF, Murata 0805 SMD Monolith 11 pF, Murata 0805 SMD Monolith 9 pF, Xicon 0805 Ceramic Chip 1 pF, AVX 0603 SMD Microwave Thin-F 0.4 pF, Dielectric Laboratories 0.7 pF, Vishay/Dale 1008 SMD Ind 68 nH, KOA Speer SMD Ind 72 nH, and Vishay/Dale High Current 1.2 μH. Surface mount chip components are used in the proposed matching circuit due to the compactness and implementation

simplicity. As compared to the distributed and complicated layout in [22], the present HF matching network is beneficial especially when the space-saving and time-saving (optimization iterations are reduced) designs are concerned.

Fig. 11 shows the measured $|S_{11}|$ of the slot-loop antenna with the filter-type impedance matching circuit, where the photograph of the matching circuit is inserted. Please note that matching circuit was connected to the antenna in the measurement and the introduced electrical length between these two is negligible at such a low frequency (HF). The simulated result is included for comparison. Note that the calculated double resonances are decreased to a single resonance in the experiment. This is ascribed to the lowered inter-coupling between resonators and might be resulted from the tolerance of lumped-element values in the matching circuit. In addition, as mentioned previously, bandwidth is broadened due to the degraded quality factor from fabrication error. Most importantly, the instantaneous bandwidth is enlarged significantly as shown in Fig. 11, where the set of antenna $|S_{11}|$ with the *L*-section and filter-type impedance matching circuits are compared. Note that the higher resonant frequency is obtained for the antenna with the filter-type impedance matching network. This is a consequence of the addition of a shunt inductance to the resonant antenna in order for wider fractional bandwidth implementation. The impedance bandwidth is improved from 0.38% (*L*-section circuit) to 1.78% (filter-type circuit) due to the employment of the filter-type matching circuit. The assembly of the miniaturized slot-loop antenna with the proposed impedance matching network demonstrates a wider impedance match of 1.78% while requiring a small area $0.031\lambda_o \times 0.017\lambda_o$, where λ_o is the free space wavelength at operational frequency.

Radiation patterns of this antenna are calculated and shown in Fig. 8 as well. Compared to the antenna with the *L*-section matching network, reduced radiation efficiency in Fig. 9 is observed for the antenna employing the filter-type matching network. This calculated efficiency η_r= 0.07 is further degraded from the previous antenna with η_r= 0.08. Although ideal lumped elements are modeled in simulation, it should be noted that current discontinuity due to the increased number of lumped elements in the matching network (the filter-type circuit) will lead to a higher conductor loss as compared to the antenna with a simpler matching network (the *L*-section circuit). The inference of dense current distribution around the filter-type matching network is observed in the full-wave

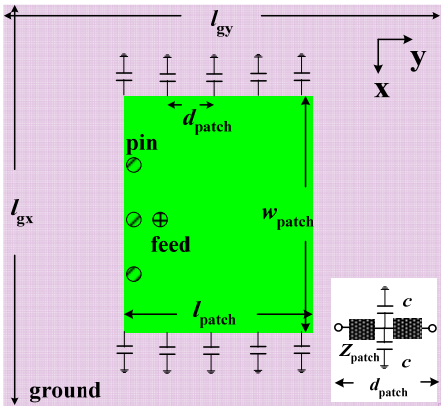

Fig. 12. The configuration of the proposed capacitor-loaded PIFA with an inset of its unit-cell model.

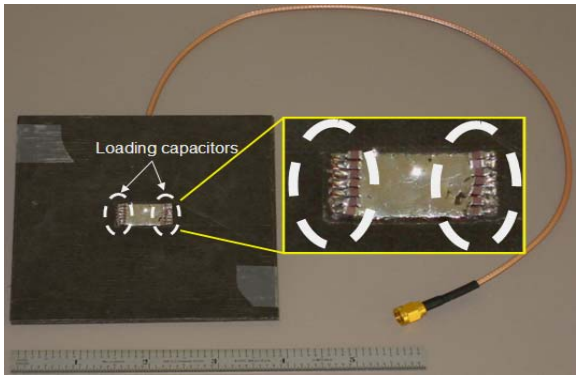

Fig. 14. Photograph of the fabricated capacitor-loaded PIFA.

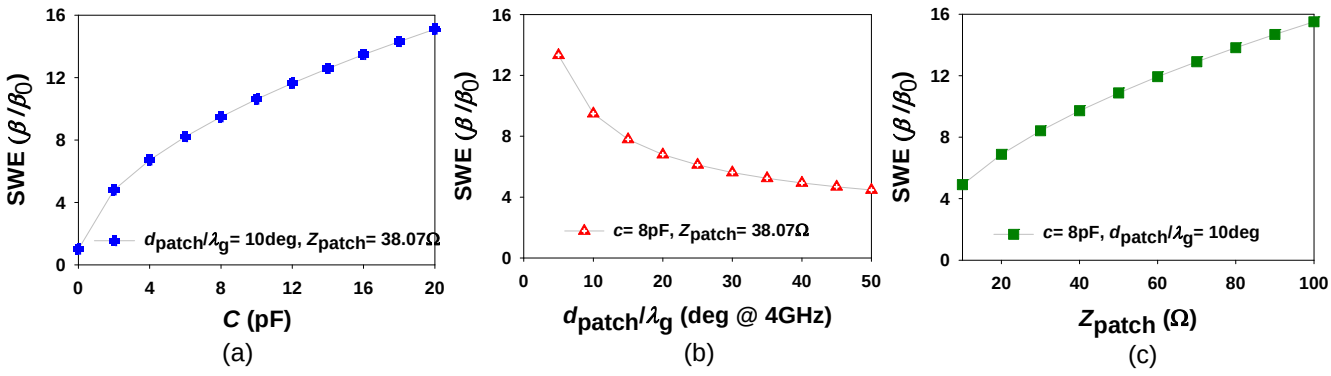

Fig. 13. SWE investigation for the capacitor-loaded PIFA (a) SWE vs. load capacitance (b) SWE vs. load period (c) SWE vs. characteristic impedance of the microstrip line.

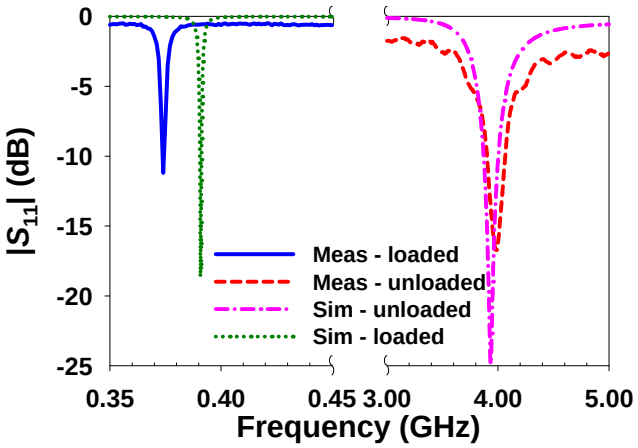

Fig. 15. Measured and calculated $|S_{11}|$ for the loaded and unloaded PIFAs.

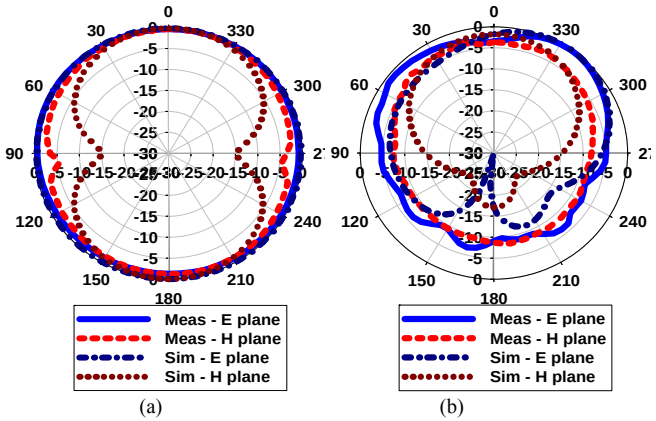

Fig. 16. Measured and calculated radiation patterns for the (a) loaded and (b) unloaded PIFAs.

simulation.

C. The Capacitor-Loaded and Miniaturized PIFA

In this subsection, a loaded and miniaturized PIFA is given as an example based on the SWE design methodology. The antenna prototype used for miniaturization is a $\lambda/4$ patch with shorting pins connected to the bottom ground plane of the substrate at one end. Applying the microstrip line model to this patch, the characteristic impedance Z_{patch} of the equivalent transmission line can be determined by the geometrical and material parameters of the patch. In addition, shunt capacitors are mounted in parallel along the longitudinal direction. Fig. 12 depicts the configuration of the proposed capacitor-loaded PIFA with its unit-cell model. The SWE as functions of the load capacitance c, load period d_{patch}/λ_g, and host-line characteristic impedance Z_{patch} was investigated using the unit-cell model and shown in Fig. 13. Each SWE curve is obtained by a respective parameter sweep when the other two are fixed as indicated in legend. The cross, triangle, and square symbols are associated with the load capacitance sweep, load period sweep, and host line characteristic impedance sweep, respectively. As before, the SWE increases when the structure is increasingly loaded (with increased load capacitance or decreased load period). Furthermore, the SWE increases with the host characteristic impedance. The combination of shunt capacitance c= 8 pF, d_{patch}/λ_g= 10 degrees at 4 GHz (1.5 mm), and Z_{patch}= 38.07 Ω provides a SWE of 9.485 and is chosen for implementation.

Fig. 14 shows the photograph of the fabricated loaded PIFA fed by a coaxial cable. The loaded antenna was built on a Rogers RT/Duroid 5880 substrate with ε_r=2.2 and thickness 3.175 mm. The Murata 0805 SMD Monolith 8 pF shunt capacitors are mounted laterally in the direction of $\lambda/4$ resonance. The dimensions for this slow wave PIFA are as follows (see Fig. 12): l_{patch}= 10.3 mm, w_{patch}= 14.82 mm, d_{patch}= 1.5 mm, and l_{gx}= l_{gy}= 50 mm. Please note that the loaded PIFA has identical dimensions as the unloaded PIFA, except loaded by capacitors. The measurement was taken with the Anritsu MS2034A vector network analyzer. Fig. 15 depicts the measured and simulated $|S_{11}|$ for both the loaded and unloaded antennas. The experimental results show good agreement with the simulated data. The unloaded PIFA has a measured $|S_{11}|$ of -16.7 dB at 3.98 GHz with a fractional bandwidth 4.07% for VSWR≤ 2 while the $|S_{11}|$ of the loaded PIFA is -11.2 dB at 0.374 GHz with a fractional bandwidth 0.15%. The significantly reduced bandwidth is the typical feature of electrically small antennas. Moreover, the measured impedance bandwidths for both cases are wider than the simulated results. In other words, a lowered quality factor is resulted from the experiment and may be ascribed to the extra loss from the fabrication error. The skewed $|S_{11}|$ response at around 0.4 GHz may be ascribed to two reasons. First, the experimental period of the capacitors placement may be less than that (1.5 mm) in simulation, which increases the miniaturization factor due to a heavier loading. Second, the tolerance from the shunt capacitors will also lead to a resonance frequency shift. As observed from the responses, the $\lambda/4$ resonant frequency was effectively reduced from the 3.98 GHz to 0.374 GHz, which shows a size reduction of 10.6. The loaded PIFA occupies a small footprint of $0.013\lambda_0 \times 0.018\lambda_0$ at 0.374 GHz. The excellent approximation to experimental miniaturization verifies the effectiveness of using the circuit-based SWE for loaded and miniaturized antenna designs. Furthermore, normalized radiation patterns of the proposed loaded and unloaded PIFAs were measured and compared to the calculated results in Fig. 16. Good agreement is observed. The E and H principal planes of this antenna are parallel to the yz and xz planes in Fig. 12 respectively. Note that the shielding effect on the backward radiation is reduced notably in the loaded situation since the electrical size of the ground plane is shrunk accordingly with operating frequency reduction. In order to prevent radiation from the coaxial cable, the ferrite beads were connected to prevent current flowing on the cable. The measured maximum radiation gain for this loaded antenna is -22.6 dBi, which is accurately predicted in the full-wave simulation with a peak radiation gain of -24.1 dBi (η_r= 0.0024). The measurement accuracy for the small antennas might have

contributed to the gain deviation. As mentioned previously, though ferrite beads were used during the measurement, there still can be some that leaks through the cable. Moreover, the broadening of the $|S_{11}|$ response might contribute to additional radiation gain. In addition, this loaded antenna is operating near the performance edge of our chamber (400 MHz). The calculated radiation efficiency of the loaded PIFA is also shown in Fig. 9 and it drops significantly compared to the loaded slot-loop antenna. This can be attributed to the significant conductor loss associated with the PIFA, which has much higher current density on the small patch.

IV. Conclusion

In the present paper, two antennas are significantly miniaturized using slow wave structures obtained by periodically loading shunt capacitors. Implementation is accelerated by employing those load parameters leading to a SWE for the desired size reduction. The experimental data show that the electrical sizes of the loaded and matched antennas are reduced to one-eleventh of their respectively unloaded counterparts. The radiation capability and impedance bandwidth, however, degrade rapidly for both antennas. The predicted antenna gain and measured bandwidth for the loaded slot loop are -34.9 dBi and 0.38% at 24 MHz, respectively. The further implementation of the proposed filter-type matching circuit on the loaded slot loop improves the bandwidth to 1.78% and meanwhile, the entire structure occupies a small footprint of $0.031\lambda_o \times 0.017\lambda_o$, where λ_o is the free space wavelength at operational frequency. In addition, the measured radiation gain and bandwidth are reduced to -22.6 dBi and 0.15%, respectively, for the electrically very small PIFA with a footprint of $0.013\lambda_0 \times 0.018\lambda_0$ at the operational frequency. Measured results validate the efficiency of the proposed design approach.

Acknowledgment

We gratefully acknowledge the support of, and technical discussions with, Diana Arceo, John Rockway and Jeff Allen from SPAWAR, San Diego.

References

[1] T. K. Lo, C. –O. Ho, Y. Hwang, E. K. W. Lam, and B. Lee, "Miniature aperture-coupled microstrip antenna of very high permittivity," *Electron. Lett.*, vol. 33, no. 1, pp. 9-10, January 1997.

[2] K. Hettak and G. Y. Delisle, "A novel reduced size CPW-coupled patch antenna topology for millimeter waves applications," in *IEEE AP-S Int. Symp.*, June 20-25, 2004, pp. 3840-3843.

[3] K. W. Leung and K. M. Luk, "Circular dielectric resonator antenna of high dielectric constant for low-profile applications," in *IEE Antennas and Propag. Conf.*, April 4-7, 1995, pp. 517-519.

[4] Y. Shirakata, N. Hidaka, M. Ishitsuka, A. Teramoto, and T. Ohmi, "High permeability and low loss Ni-Fe composite material for high-frequency applications," *IEEE Trans. Magn.*, vol. 44, no. 9, pp. 2100-2106, September 2008.

[5] Z. Chen, T. See, and X. Qing, "Ultra-wideband antennas with miniaturized size, reduced ground plane reliance, and enhanced diversity," in *IEEE iWAT Int. Workshop*, March 4-6, 2008, pp. 24-27.

[6] A. Djaiz, T. Denidni, and M. Nedil, "A new CPW-feed miniaturized antenna with bandwidth enhancement for biomedical localization applications," in *IEEE AP-S Int. Symp.*, June 9-15, 2007, pp. 5439-5442.

[7] G. Mumcu, K. Sertel, and J. L. Volakis, "Miniature antenna using printed coupled lines emulating degenerate band edge crystals," *IEEE Trans. Antennas and Propag.*, vol. 57, no. 6, pp. 1618-1624, June 2009.

[8] C. –J. Lee, K.M. K. H. Leong, and T. Itoh, "Compact dual-band antenna using an anisotropic metamaterial," in *Proc. 36th Eur. Microw. Conf.*, September 10-15, 2006, pp. 1044-1047.

[9] —, "Composite right/left-handed transmission line based compact resonant antennas for RF module integration," *IEEE Trans. Antennas and Propag.*, vol. 54, no. 8, pp. 2283-2291, August 2006.

[10] N. Behdad and K. Sarabandi, "Bandwidth enhancement and further size reduction of a class of miniaturized slot antennas," *IEEE Trans. Antennas Propag.*, vol. 52, no. 8, pp. 1928-1935, August 2004.

[11] C. Chiu, K. Shum, and C. Chan, "A tunable via-patch loaded PIFA with size reduction," *IEEE Trans. Antennas Propag.*, vol. 55, no. 1, pp. 65-71, January 2007.

[12] C. Rowell and R. Murch, "A capacitively loaded PIFA for compact mobile telephone handsets," *IEEE Trans. Antennas Propag.*, vol. 45, no. 5, pp. 837-842, May 1997.

[13] R. Azadegan and K. Sarabandi, "A novel approach for miniaturization of slot antennas," *IEEE Trans. Antennas Propag.*, vol. 51, no. 3, pp. 421-429, March 2003.

[14] F. -R. Yang, K. -P. Ma, Y. Qian, and T. Itoh, "A uniplanar compact photonic-bandgap (UC-PBG) structure and its applications for microwave circuits," *IEEE Trans. Microw. Theory Tech.*, vol. 47, no. 8, pp. 1509-1514, August 1999.

[15] J. –S. Chen, "Triple-frequency annular-ring slot antennas fed by CPW and microstrip line," in *IEEE AP-S Int. Symp.*, June 22-27, 2003, pp. 557-560.

[16] W. –S. Chen and K. –L. Wong, "A compact waveguide-fed printed slot antenna for dual-frequency operation," in *IEEE AP-S Int. Symp.*, July 8-13, 2001, pp. 140-143.

[17] G. Forma and J. M. Laheurte, "Compact oscillating slot loop antenna with conductor backing," *Electron. Lett.*, vol. 32, no. 18, pp. 1633-1635, August 1996.

[18] N. Lenin and P. H. Rao, "Broadband printed square slot loop antenna," in *IEEE AP-S Int. Symp.*, July 3-8, 2005, pp. 557-560.

[19] P. -L. Chi, K. Leong, R. Waterhouse, and T. Itoh, "A miniaturized CPW-fed capacitor-loaded slot-loop antenna," in *IEEE ISSSE Int. Symp.*, July 30- August 2, 2007, pp. 595-598.

[20] M. Lee, B. A. Kramer, C. –C. Chen, and J. L. Volakis, "Distributed lumped loads and lossy transmission line model for wideband spiral antenna miniaturization and characterization," *IEEE Trans. Antennas and Propag.*, vol. 55, no. 10, pp. 2671-2678, October 2007.

[21] G. L. Matthaei, L. Young, and E. M. T. Jones, *Microwave Filters, Impedance- Matching Networks, and Coupling Structures*, Section 8.03, Section 11.08, McGraw-Hill, 1964.

[22] Y. Tsutsumi, H. Kanaya, and K. Yoshida, "Design and performance of an electrically small slot loop antenna with a miniaturized superconducting matching circuit," *IEEE Trans. Applied Superconductivity*, vol. 15, no. 2, pp. 1020-1023, June 2005.

[23] K. C. Gupta, R. Garg, I. Bahl, and P. Bhartia, *Microstrip Lines and Slotlines*, 2nd ed., Artech House, 1996.

[24] D. M. Pozar, *Microwave Engineering*, 2nd ed., John Wiley & Sons, 1998.

[25] R. Janaswamy and D. H. Schaubert, "Characteristic impedance of a wide slotline on low-permittivity substrates," *IEEE Trans. Microw. Theory Tech.*, vol. 34, no. 8, pp. 900-902, August 1986.

[26] W. L. Stutzman and G. A. Thiele, *Antenna Theory and Design*, 2nd ed., Chapter 5, pp. 215, New York: Wiley, 1998.

[27] M. –C. Huynh and W. Stutzman, "Ground plane effects on planar inverted-F antenna (PIFA) performance," *IEE Proc. Microw. Antennas Propag.*, vol. 150, no. 4, August 2003.

[28] W. Tan, Z. Shen, and Z. Shao, "Radiation of high-gain cavity-backed slot antennas through a two-layer superstrate," *IEEE Antennas and Propag. Mag.*, vol. 50, no. 3, pp. 78-87, June 2008.

[29] H. Vettikalladi, O. Lafond, and M. Himdi, "High-efficient and high-gain superstrate antenna for 60-GHz indoor communication," *IEEE Antennas and Wireless Propag. Lett.*, vol. 8, pp. 1422-1425, 2009.

[30] C. –Y. Huang, J. –Y. Wu, and K. –L. Wong, "High-gain compact circularly polarized microstrip antenna," *Electron. Lett.*, vol. 34, no.8, pp. 712-713, April 1998.

[31] Raven Research, Model No. RR6309, www.raven-research.com.

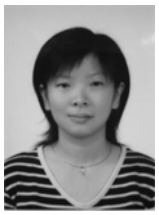

Pei-Ling Chi (S'08) received the B.S. and M.S. degrees in Communication Engineering from the National Chiao Tung University (NCTU), Hsinchu, Taiwan, R.O.C. in 2004 and 2006 respectively, and is currently working toward the Ph.D. degree in the department of electrical engineering, University of California at Los Angeles (UCLA).

Her research interests include the analysis and design of antennas and microwave circuits.

Rod Waterhouse (S'90-M'92-SM'01) received his BEng, MS, and PhD in Electrical Engineering from the University of Queensland, Australia, in 1987, 1989 and 1994, respectively. In 1994 he joined RMIT University as a lecturer and become a Senior Lecturer in 1997 and an Associate Professor in 2002. From 2001 - 2003 Dr Waterhouse was with the venture-backed Dorsal Networks which was later acquired by Corvis Corporation. In 2004 he co-founded Pharad, an antenna and wireless communications company, where he is now Vice President. He is also a Senior Fellow within the Department of Electrical and Electronic Engineering at the University of Melbourne. Dr Waterhouse's research interests include antennas, electromagnetics and microwave photonics engineering. He has over 260 publications in these fields, including 2 books and 4 book chapters. Dr Waterhouse is an associate Editor for the IEEE Transactions on Antennas and Propagations. He chaired the IEEE Victorian MTTS/APS Chapter from 1998 - 2001 and in 2000 received an IEEE Third Millennium Medal for Outstanding Achievements and Contributions.

Tatsuo Itoh (S'69-M'69-SM'74-F'82-LF'06) received the Ph.D. Degree in Electrical Engineering from the University of Illinois, Urbana in 1969. From September 1966 to April 1976, he was with the Electrical Engineering Department, University of Illinois. From April 1976 to August 1977, he was a Senior Research Engineer in the Radio Physics Laboratory, SRI International, Menlo Park, CA. From August 1977 to June 1978, he was an Associate Professor at the University of Kentucky, Lexington. In July 1978, he joined the faculty at The University of Texas at Austin, where he became a Professor of Electrical Engineering in 1981 and Director of the Electrical Engineering Research Laboratory in 1984. During the summer of 1979, he was a guest researcher at AEG-Telefunken, Ulm, West Germany. In September 1983, he was selected to hold the Hayden Head Centennial Professorship of Engineering at The University of Texas. In September 1984, he was appointed Associate Chairman for Research and Planning of the Electrical and Computer Engineering Department at The University of Texas. In January 1991, he joined the University of California, Los Angeles as Professor of Electrical Engineering and holder of the TRW Endowed Chair in Microwave and Millimeter Wave Electronics (currently Northrop Grumman Endowed Chair). He was an Honorary Visiting Professor at Nanjing Institute of Technology, China and at Japan Defense Academy. In April 1994, he was appointed as Adjunct Research Officer for Communications Research Laboratory, Ministry of Post and Telecommunication, Tokyo, Japan. He currently was Visiting Professor at University of Leeds, United Kingdom. He received a number of awards including Shida Award from Japanese Ministry of Post and Telecommunications in 1998, Japan Microwave Prize in 1998, IEEE Third Millennium Medal in 2000, and IEEE MTT Distinguished Educator Award in 2000. He was elected to a member of National Academy of Engineering in 2003.

Dr. Itoh is a Fellow of the IEEE, a member of the Institute of Electronics and Communication Engineers of Japan, and Commissions B and D of USNC/URSI. He served as the Editor of IEEE Transactions on Microwave Theory and Techniques for 1983 - 1985. He serves on the Administrative Committee of IEEE Microwave Theory and Techniques Society. He was Vice President of the Microwave Theory and Techniques Society in 1989 and President in 1990. He was the Editor-in-Chief of IEEE Microwave and Guided Wave Letters from 1991 through 1994. He was elected as an Honorary Life Member of MTT Society in 1994. He was the Chairman of USNC/URSI Commission D from 1988 to 1990, and Chairman of Commission D of the International URSI for 1993 - 1996. He was Chair of Long Range Planning Committee of URSI. He serves on advisory boards and committees of a number of organizations. He served as Distinguished Microwave Lecturer on Microwave Applications of Metamaterial Structures of IEEE MTT-S for 2004 – 2006.

He has 375 journal publications, 775 refereed conference presentations and has written 43 books/book chapters in the area of microwaves, millimeter-waves, antennas and numerical electromagnetics. He generated 68 Ph.D. students.